View metadata, citation and similar papers at core.ac.uk

brought to you by CORE

provided by CURVE/open

A plasticity constitutive model for unsaturated, anisotropic, nonexpansive soils

Sitarenios, P. & Kavvadas, M.

Author post-print (accepted) deposited by Coventry University's Repository

Original citation & hyperlink:
Sitarenios, P & Kavvadas, M 2020, 'A plasticity constitutive model for unsaturated, anisotropic, nonexpansive soils', International Journal for Numerical and Analytical Methods in Geomechanics, vol. 44, no. 4, pp. 435-454.
https://dx.doi.org/10.1002/nag.3028

DOI 10.1002/nag.3028
ISSN 0363-9061
ESSN 1096-9853

Publisher: Wiley

This is the peer reviewed version of the following article: Sitarenios, P & Kavvadas, M 2020, 'A plasticity constitutive model for unsaturated, anisotropic, nonexpansive soils', International Journal for Numerical and Analytical Methods in Geomechanics, vol. 44, no. 4, pp. 435-454 which has been published in final form at https://dx.doi.org/10.1002/nag.3028 This article may be used for non-commercial purposes in accordance with Wiley Terms and Conditions for Self-Archiving.

Copyright © and Moral Rights are retained by the author(s) and/ or other copyright owners. A copy can be downloaded for personal non-commercial research or study, without prior permission or charge. This item cannot be reproduced or quoted extensively from without first obtaining permission in writing from the copyright holder(s). The content must not be changed in any way or sold commercially in any format or medium without the formal permission of the copyright holders.

This document is the author's post-print version, incorporating any revisions agreed during the peer-review process. Some differences between the published version and this version may remain and you are advised to consult the published version if you wish to cite from it.

ORIGINAL ARTICLE

A plasticity Constitutive Model for Unsaturated, Anisotropic, non-expansive soils (CMUA)

Sitarenios Panagiotis, Lecturer in Civil Engineering - Geotechnics[1]* | Kavvadas Michael, Professor of Civil Engineering[2]†

[1]School of Energy, Construction and Environment, Coventry University, UK. Former affiliation: Geotechnical Department, School of Civil Engineering, National Technical University of Athens, Greece

[2]Geotechnical Department, School of Civil Engineering, National Technical University of Athens, Greece

Correspondence
School of Energy, Construction and Environment, Sir John Laing Bldg., Coventry University, CV1 5FB, Coventry, UK
Email: panagiotis.sitarenios@coventry.ac.uk

Funding information

The paper describes and evaluates an incremental plasticity constitutive model for anisotropic, unsaturated, non-expansive soils (CMUA). It is based on the Modifed Cam-Clay (MCC) model for saturated soils and enhances it by introducing anisotropy (via rotation of the MCC yield surface) and an unsaturated compressibility framework describing a double dependence of compressibility on suction and on the degree of saturation of macro-porosity. As the anisotropic and unsaturated features can be activated independently, the model is downwards compatible with the MCC model. The CMUA model can simulate effectively: the dependence of compressibility on the level of developed anisotropy; uniqueness of critical state independent of the initial anisotropy; an evolving compressibility during constant suction compression; and a maximum of collapse. The model uses Bishop's average skeleton stress as its first constitutive variable, favoring its numerical implementation in commercial numerical analysis codes (e.g., finite element codes) and a unified treatment of saturated and unsaturated material states.

KEYWORDS
critical state plasticity, soil anisotropy, unsaturated soils, constitutive model, Bishop's stress

1 | INTRODUCTION

Since the proposal of the first complete constitutive model for unsaturated soils, the Barcelona Basic Model (BBM) by Alonso et al. [4], various constitutive models have been proposed to capture the behaviour of unsaturated soils. Most of the researchers build on the Critical State Soil Mechanics theory [37], by extending the Modified Cam Clay (MCC) model [36] to account for the behaviour of partially saturated material elements.

The BBM model utilizes net stress and suction as its first (FCV) and second constitutive variable (SCV), respectively. In BBM, the MCC compressibility framework was extended for unsaturated material states by incorporating suction dependant virgin Compression Lines (CLs) to describe a reducing compressibility with increasing suction. By further relating the preconsolidation pressure under saturated conditions with the apparent preconsolidation pressure developing with an increase in suction, the Loading-Collapse (LC) surface was introduced. The LC surface is a yield surface, bounding the elastic domain in the net stress ($\overline{\boldsymbol{\sigma}}$) - suction s plane and describes in a unified way irreversible volume reduction associated with loading under constant suction together with wetting under constant net stress (collapse). Until nowadays, the LC concept comprises the most fundamental idea in constitutive modelling of unsaturated soils.

Various researchers tried to enhance BBM's capabilities to reproduce a maximum of collapse with wetting [26, 23], a non-linear evolution of shear strength with suction [23, 7] and also a stabilization of void ratio around a minimum value during drying [7, 38]. However, the main shortcoming of net stress formulation is that it requires special handling when it comes to numerical analyses as it cannot recover Terzaghi's effective stress upon saturation and thus hinders the unified analyses of saturated and unsaturated materials states.

This fact motivated researchers to replace net stress with Bishop's average skeleton stress [9] as a constitutive variable. Following early attempts by Kohgo et al. [31] and Bolzon et al. [10], Jommi [25] studied in detail constitutive modelling of unsaturated soils through Bishop's stress. The author incorporated Bishop's stress in the yield equation of the MCC and compared the reproduced behaviour with the BBM framework. This comparison revealed that the behaviour in the elastic domain as well as the non-linear increase in shear strength with suction are a natural outcome of Bishop's stress implementation while, to the contrary, the increase in the apparent preconsolidation pressure with partial saturation still calls for extra constitutive equations and additional constitutive variables.

In that respect, various researchers [27, 35, 42, 24] utilized suction as their additional, second constitutive variable. Such an approach has the shortcoming that it necessitates the definition of a discontinuous evolution of the unsaturated compressibility with suction to ensure that fully saturated material states (e.g., suction levels below the desaturation suction) do not deviate from the compression line of the saturated material. A more recent approach suggests the utilization of degree of saturation as an extra constitutive variable, with suction contributing only indirectly through Bishop's stress definition and through the Water Retention Curve (WRC). Different approaches with respect to the evolution of compressibility with partial saturation exist. For instance, Zhou et al. [48] adopted a constantly decreasing slope for the CLs with decreasing S_r, while other researchers [30, 47, 13] assume a parallel translation of the CLs towards higher void ratio values. Contributions where suction and degree of saturation are combined into a single parameter also exist [20, 45, 5], while recently Gallipoli and Bruno [19] proposed the "scaled stress" concept, a stress variable based on Bishop's stress, which seems capable of unifying the mechanical behaviour of saturated and unsaturated soils within a single constitutive variable.

Existing constitutive models cover a wide spectrum of the mechanical and hydraulic behavioural characteristics of unsaturated soils. However, one of the issues that has not drawn significant attention is the combination of partial saturation with soil anisotropy, an issue of significant importance given the fact that in practical applications partial saturation usually concerns either compacted or 1D consolidated soils, both exhibiting strong evidence of anisotropy. Cui

and Delage [14] had emphasized on the fact that the yield surface of anisotropically consolidated soil elements under unsaturated conditions is not isotropic, in line with the behaviour exhibited by their saturated counterparts. Thus, they suggested the adoption of anisotropic constitutive models [28, 46, 44, 15] as the saturated reference for the development of unsaturated constitutive models. Following Cui and Delage [14], Stropeit et al. [41] extended the S-CLAY1 [44] anisotropic critical state model into the unsaturated regime by incorporating the BBM framework. Their model was further enhanced by D'Onza et al. [18] and Al-Sharrad and Gallipoli [2] with an eye towards improved shear strength predictions and improved yield stress and shear strains prediction in the former and the latter contribution respectively. The common denominator of the aforementioned contributions is their net stress formulation, while according to the authors' knowledge no contributions utilizing Bishop's stress exist.

The present paper tries to fill this gap in the state of the art by proposing an anisotropic constitutive model for unsaturated material states utilizing Bishop's average skeleton stress. The proposed model builds on the Kavvadas [28] MIT-E1 anisotropic constitutive model for saturated material states, enhances its anisotropic capabilities by modifying its flow and hardening rules and then extends it into the unsaturated regime using a compressibility framework proposed by the authors [40]. The proposed new Constitutive Model for Unsaturated, Anisotropic soils (CMUA) is a single yield surface model which incorporates a distorted ellipsoid as its yield surface, a non-associated flow rule based on a plastic potential surface with a similar shape but different orientation with respect to the yield surface and a mixed (kinematic and isotropic) hardening rule. A Loading - Collapse surface is incorporated based on a compressibility framework which describes compression lines dependant both on suction and degree of saturation. The CMUA model is evaluated through parametric analyses and also calibrated against available experimental results. The presented simulations prove that the model is capable of predicting distinct and parallel compression lines depending on the level of anisotropy, unique critical state irrespective of the initial level of anisotropy and of the stress path followed, an evolving compressibility for compression under constant suction as well as a maximum of collapse. It also reveals shortcomings of the proposed formulation which need to be addressed in future updates.

2 | MODEL FORMULATION

The proposed constitutive model builds on the classical, rate-independent (inviscid) theory of elasto-plasticity. In the proposed model's constitutive equations, only Bishop's stress appears and thus for simplicity it is simple denoted as $\boldsymbol{\sigma}$, with primes dropped to avoid potential misunderstanding that Bishop's average skeleton stress comprises an effective stress quantity. Net stress appears in the Bishop's stress definition and also in some graphs and will be symbolized as $\overline{\boldsymbol{\sigma}}$. Finally, a bold symbol indicates a tensorial quantity (i.e., $\boldsymbol{\sigma}$), dot over a symbol (i.e., $\dot{\boldsymbol{\sigma}}$) denotes an infinitesimal increment of the aforementioned quantity and the symbol ":" indicates a summation of the products over all tensorial indices.

In the generalized stress space, we assume the following Bishop's average skeleton stress definition:

$$\boldsymbol{\sigma} = \overline{\boldsymbol{\sigma}} + s \cdot S_r^e \cdot \boldsymbol{I} \tag{1}$$

where net stress $\overline{\boldsymbol{\sigma}}$ is the excess of total stress over the pressure of the air phase: $\overline{\boldsymbol{\sigma}} = \boldsymbol{\sigma}_{tot} - u_a \cdot \boldsymbol{I}$. Comparison of equation 1 with the original Bishop's stress definition [9] reveals that the CMUA model uses the effective or macro-structural degree of saturation (S_r^e) as its scaling parameter (χ). In fact, the model subscribes to the idea of Alonso et al. [3] suggesting that in common non-expansive soils which develop a double porosity (e.g., clayey soils), the mechanical behaviour is dominated by the water contained in the larger macropores. To scale degree of saturation

for macrostuctural effects, the present paper adopts the simple power law of Alonso et al. [3]:

$$S_r^e = (S_r)^\alpha \tag{2}$$

where parameter α is a material constant. It must be calibrated for each soil individually and is expected to increase with an increase in fines. Bishop's stress tensor can be decomposed to an isotropic and a deviatoric part following:

$$p = \frac{1}{3}\boldsymbol{\sigma} : \boldsymbol{I} = \frac{1}{3}\overline{\boldsymbol{\sigma}} : \boldsymbol{I} + s \cdot S_r^e \tag{3a}$$

$$\boldsymbol{s} = \boldsymbol{\sigma} - p\boldsymbol{I} \tag{3b}$$

2.1 | Elasticity

The model follows the basic kinematic assumption of the additive decomposition of the total strain increment in an elastic $\dot{\boldsymbol{\varepsilon}}^{\mathbf{e}}$ and a plastic (irreversible) $\dot{\boldsymbol{\varepsilon}}^{\mathbf{p}}$ part ($\dot{\boldsymbol{\varepsilon}} = \dot{\boldsymbol{\varepsilon}}^e + \dot{\boldsymbol{\varepsilon}}^p$). The elastic strain increment is computed through the elastic law for which the proposed model adopts the MCC porous elastic behaviour. Poroelasticity is an isotropic linear elastic law where the Bulk Modulus K and the Shear Modulus G are computed as:

$$K = \frac{vp}{\kappa} \tag{4a}$$

$$G = \frac{3(1-2\nu)}{2(1+\nu)}K \tag{4b}$$

where κ the MCC parameter representing the slope of the swelling lines in the $v - \ln p$ plane, $v = 1 + e$ the specific volume and ν as Poisson's ratio. Bishop's average skeleton stress, combined with the MCC porous elastic behaviour, can sufficiently represent elastic straining in unsaturated media and thus, no further assumptions are needed to represent the elastic behaviour due to changes in suction or degree of saturation. Finally, an increment of stress is associated with an elastic strain increment through:

$$\dot{\boldsymbol{\sigma}} = \boldsymbol{C}^{\mathbf{e}} : \dot{\boldsymbol{\varepsilon}}^e \Rightarrow \begin{Bmatrix} \dot{p} \\ \dot{\boldsymbol{s}} \end{Bmatrix} = \begin{pmatrix} K & \mathbf{0} \\ \mathbf{0} & 2G \end{pmatrix} : \begin{Bmatrix} \dot{\varepsilon}_v^e \\ \dot{\boldsymbol{e}}^e \end{Bmatrix} \tag{5}$$

where $\dot{\varepsilon}_v^e$ the elastic volumetric strain increment and $\dot{\boldsymbol{e}}^e$ the tensor of elastic deviatoric strain increments, both following the decomposition of the strain tensor to an isotropic and a deviatoric part according to:

$$\varepsilon_v = \boldsymbol{\varepsilon} : \boldsymbol{I} \tag{6a}$$

$$\boldsymbol{e} = \boldsymbol{\varepsilon} - \frac{1}{3}\varepsilon_v \boldsymbol{I} \tag{6b}$$

For simplicity of the formulation and also for limiting the number of parameters the model does not account for the effect of anisotropy in the elastic behaviour. Such a selection is further supported from experimental evidence suggesting that the effect of anisotropy in the elastic domain is limited [1].

2.2 | Plastic Yield Envelope (PYE)

The proposed model incorporates a single yield surface, which serves as a Plastic Yield Envelope (PYE), differentiating between elastic and elastoplastic stress states. The incorporated yield surface takes into account both the effects of anisotropy and partial saturation. In the following lines the adopted yield surface is introduced progressively through characteristic surfaces corresponding to reference states. Initially, the Saturated Yield Envelope (SatYE) is introduced, which as the name implies corresponds to the model's yield surface under saturated conditions. Then, the adopted unsaturated compressibility framework is described and utilized in deriving the Unsaturated Yield Envelope (UnsatYE). The model's yield surface coincides with the UnsatYE envelope, while upon saturation reduces to the SatYE.

2.2.1 | Saturated Yield Envelope

The proposed model adopts the distorted ellipsoid proposed by Kavvadas [28] to account for the yield locus of anisotropically consolidated saturated soil elements. In the generalized stress space it takes the following form:

$$F(p, \boldsymbol{s}, p_0, \boldsymbol{b}) = \frac{1}{k^2}(\boldsymbol{s} - p\boldsymbol{b}) : (\boldsymbol{s} - p\boldsymbol{b}) - p(p_0 - p) \tag{7}$$

where p_0 controls the size of the ellipsoid and comprises the isotropic hardening variable of the model, $\boldsymbol{b}$ is the kinematic hardening variable tensor controlling the orientation of the Saturated Yield Envelope in all deviatoric planes, and; k a material constant defining the ratio of the axes of the ellipsoid.

Figure 1a presents the adopted ellipsoid in the tensorial stress space consisting from the hydrostatic axis and the deviatoric stress hyperspace. The same figure additionally includes a secondary characteristic surface corresponding to isotropic reference states. It is an ellipsoid identical to the MCC yield surface, given by the following equation:

$$F^*(p, \boldsymbol{s}, p_0^*) = \frac{1}{k^2}\boldsymbol{s} : \boldsymbol{s} - p(p_0^* - p) \tag{8}$$

where p_0^* a scalar variable corresponding to the size of the isotropic ellipsoid. The SatYE reduces to the Intrinsic Isotropic Envelope when the anisotropy tensor is null ($\boldsymbol{b} = \boldsymbol{0}$ and $p_0 = p_0^*$).

Leroueil and Vaughan [33] defined as structureless soil states those uniquely defined by the current void ratio and the current stress state, while such material states can be additionally described as Intrinsic according to Burland [11]. The MCC isotropic ellipse represents such material states and its size can be computed as:

$$p_0^* = exp\left(\frac{N_{iso} - v - \kappa \ln p}{\lambda - \kappa}\right) \tag{9}$$

where λ the MCC compressibility parameter representing the slope of the virgin compression lines in the $v - \ln p$ plane and N_{iso} defines the position of the isotropic virgin compression line in the $v - \ln p$ plane.

When an initially isotropically consolidated soil element undergoes plastic straining under anisotropic stress states (e.g., radial consolidation, oedometric compression) it gradually develops anisotropy, manifested as preferred directions in stress space. The adopted anisotropic ellipsoid follows the idea that a soil element subjected to a virgin radial stress path with direction $\boldsymbol{\beta}$ lays on the tip of a distorted yield surface with its axis oriented along the same direction. In that respect, the tip of the SatYE (p_0) represents the preconsolidation pressure of an anisotropically consolidated material.

In the $v - \ln p$ plane, the volumetric behaviour of anisotropically consolidated soil elements can be fairly approxi-

mated by a set of parallel compression lines with slope λ and position depending on the applied stress path [34, 22]. Belokas and Kavvadas [8] proposed an Intrinsic Compressibility Framework (ICF) to reproduce such a behaviour. Figure 1b shows a set of parallel compression lines representing consolidation under different stress paths.

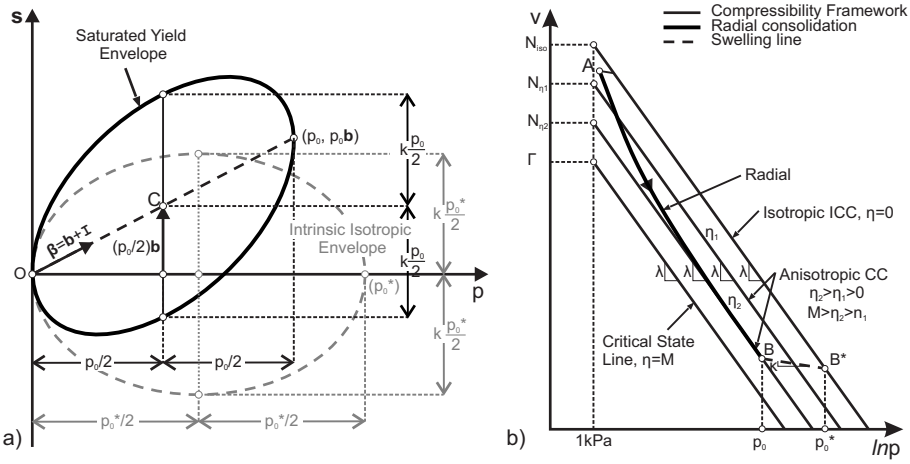

FIGURE 1 a) The Saturated Yield Envelope and the Intrinsic Isotropic Envelope in the p - $\boldsymbol{s}$ hyperspace and; b) the Belokas and Kavvadas [8] Intrinsic Compressibility Framework

They represent reference material states where the volumetric behaviour of an anisotropically consolidated stress element should lay on under stabilized anisotropic conditions (e.g., constant dilatancy reproduced). The thick line in figure 1b corresponds to such a compression path associated with an imposed radial stress path with ratio $\eta = q/p$. Point B corresponds to the preconsolidation pressure of the material and thus, represents the tip of the distorted ellipsoid. Through a proper swelling line, point B can be projected to the isotropic compression line (Point B*) with the latter corresponding to the equivalent isotropic reference state located on the Isotropic Intrinsic Envelope (p_0^*). By relating the specific volume at points B and B* through the swelling line we may compute:

$$p_0 = \exp\left(\frac{N_{iso} - N_\eta}{\kappa - \lambda}\right) p_0^* \tag{10}$$

Parameter N_n describes the position of the anisotropic compression line and depends on the level of induced anisotropy through the stress ratio $\sqrt{\boldsymbol{s} : \boldsymbol{s}/p^2}$, the later in the generalized stress space. It is computed via the following expression which is a slightly modified version of the one proposed by Belokas and Kavvadas [8].

$$N_\eta = \Gamma + (N_{iso} - \Gamma)\left(1 - \frac{\frac{1}{c^2}(\boldsymbol{s} : \boldsymbol{s})}{p^2}\right)^{r_s} \tag{11}$$

where Γ defines the position of the Critical State Line (CSL) line in the $v - \ln p$ plane and c corresponds to the slope of the CSL in each deviatoric hyperaxis and is related to the MCC parameter M ($c = \sqrt{2/3}M$). Equation 11 assumes that the upper limit of N_η is the N_{iso} value representing the Isotropic CL, while the lower limit, the Γ value, represents the CSL which according to Gens [22], corresponds to the theoretical maximum stress path ratio which reproduces a continuously hardening behaviour. Parameter r_s is a material constant and controls the spacing of intermediate

anisotropic compression lines (between N_{iso} and Γ) in the $v - \ln p$ plane.

Equations 10 & 11 relate the preconsolidation pressure of the material with the level of developed anisotropy. Combining these equations and further taking into account that under stabilized anisotropic conditions the inclination of the yield surface coincides with the stress path of the consolidation ($\sqrt{\boldsymbol{s} : \boldsymbol{s}/p^2} = \sqrt{\boldsymbol{b} : \boldsymbol{b}}$), we may simply write that:

$$p_0 = A p_0^* \tag{12}$$

where:

$$A = exp\left[\frac{\Gamma - N_{iso}}{\lambda - \kappa}\left[1 - \left(1 - \frac{1}{c^2}\boldsymbol{b} : \boldsymbol{b}\right)^{r_s}\right]\right] \tag{13}$$

2.2.2 | Unsaturated Yield Envelope

Any constitutive model can be extended into the unsaturated regime by introducing a Loading-Collapse (LC) Surface which describes the evolution of the apparent pre-consolidation pressure with partial saturation. Although many researchers postulate directly on the evolution of apparent preconsolidation pressure with partial saturation, it is more elegant to derive the LC curve from the adopted unsaturated compressibility framework, similar to BBM. The proposed model adopts and enhances the compressibility framework of Sitarenios and Kavvadas [40] which describes a double dependance of the compression lines on suction and macrostructural degree of saturation. If we examine the compressibility behaviour of an unsaturated soil element in the $v - \ln p$ plane (figure 2a), the proposed framework assumes that there exists a reference pressure p^c defining a point on the compression line of the saturated material from where different compression lines, corresponding to different states of partial saturation, originate from. Partial saturation leads to a decrease in compressibility, moving unsaturated material states to the right of the saturated compression curves in the meta-stable domain [29]. This transition in the meta-stable domain is similar to the effect that other structuring agents like cementation or thixotropy have on natural soils. In unsaturated soils, structure is attributed to the forming inter-particle bonding forces between soil grains and aggregates, mainly due to the forming water menisci. Gallipoli et al. [20] proposed that the intensity of such inter-particle forces depends both on the level of applied suction, which defines their strength, but also on the water contained in the examined soil system, represented by degree of saturation and describing the “density" of the forming forces. To represent such a behavior the authors combined the effect of suction and partial saturation to a single variable, the bonding factor (ξ), while recently Alonso et al. [6] adopted a similar idea.

The proposed framework also subscribes to the aforementioned idea, but it attempts to capture this double dependence by examining the effect of suction and degree of saturation independently. To start with the effect of suction, the proposed framework adopts the BBM compressibility equation to describe the dominant effect that an increase in suction has in reducing compressibility and thus, in stiffening the behaviour. The BBM compressibility evolution law is described by the following formula:

$$\lambda(s) = \lambda\left[(1 - r)\, e^{-\beta s} + r\right] \tag{14}$$

where β, r material constants. To further account for the effect of degree of saturation, the proposed framework adopts the following equation:

$$\lambda(s, S_r^e) = \lambda - (\lambda - \lambda(s))\left(1 - S_r^e\right)^{\gamma} \tag{15}$$

In equation 15 the macrostructural degree of saturation is incorporated and assumed to act as a “destructuring" agent. In more detail, if we consider a compression under constant suction, then an increase in degree of saturation, increases the soil's compressibility and drags the material state towards the intrinsic compression curve corresponding to saturated material states. Such a behaviour is the natural outcome of the progressive destruction of existing menisci as the water content increases. It additionally ensures that saturated material states lay on the saturated compression line, a prerequisite for Bishop's stress formulation, ensuring a continuous behaviour as the latter recalls Terzaghi's effective stress upon saturation. On the other extreme, under a relatively high suction level, the effective degree of saturation S_r^e can theoretically approach zero. In that case equation 15 reduces to the BBM compressibility and reproduces a constant unsaturated compressibility ($\lambda(s, S_r^e) \rightarrow \lambda(s)$). This limiting case corresponds to a soil state where the larger macropores are empty and the mechanical behaviour is dominated by the absorptive and osmotic phenomena contributing to soil suction.

Combining equations 14 and 15 we end up with the following expression:

$$\lambda(s, S_r^e) = \lambda \left[1 - (1 - r)\left(1 - S_r^e\right)^{\gamma} \left(1 - e^{-\beta s}\right)\right] \tag{16}$$

where parameter γ is an extra material constant scaling the effect of degree of saturation on compressibility. Note that BBM parameters β and r although they retain their initial role in controlling compressibility, they must be calibrated to available experimental results by also considering the effect of degree of saturation and the interplay with parameter γ. Equation 16 can describe a constantly increasing compressibility for compression under constant suction as a result of an increasing degree of saturation due to the increasing capacity of water retention with a reducing void ratio (e.g., stress paths ABB′ and ACC2′ in figure 2a). Such an evolving compressibility can naturally explain a maximum of collapse (e.g., wetting paths CC1′ vs CC2′ in figure 2a).

Having defined the unsaturated compressibility framework a similar procedure with the BBM model is utilized to correlate the apparent preconsolidation pressure (Point C in figure 2a) with the corresponding preconsolidation pressure under saturated conditions (Point A in figure 2a). Using a proper swelling line with slope κ, we calculate:

$$p_0(s, S_r^e) = p^c \left(\frac{p_0}{p^c}\right)^{\frac{\lambda - \kappa}{\lambda(s, S_r^e) - \kappa}} \tag{17}$$

with $\lambda(s, S_r^e)$ described through equation 16. Equation 17 represents the Loading - Collapse Curve of the proposed constitutive model and finally the unsaturated yield envelope is represented by the following yield equation:

$$f\left(p, \boldsymbol{s}, p_0\left(s, S_r^e\right), \boldsymbol{b}\right) = \frac{1}{k^2}(\boldsymbol{s} - p\boldsymbol{b}) : (\boldsymbol{s} - p\boldsymbol{b}) - p(p_0\left(s, S_r^e\right) - p) \tag{18}$$

Equations 16 to 18 describe the complete Plastic Yield Envelope (PYE) of the proposed model which is further depicted in figure 2b. It encloses all the elastic domain and for saturated material states ($S_r^e = 1.0$), $\lambda(s, S_r^e) = \lambda$ and $p_0(s, S_r^e) = p_0$ thus, it reduces to the saturated yield envelope (eq. 7). Very recently, Al-Sharrad et al. [1] suggested that the proposed ellipsoid, in the p-q space, describes satisfactory the yield locus of anisotropically consolidated, unsaturated Speswhite Kaolin samples.

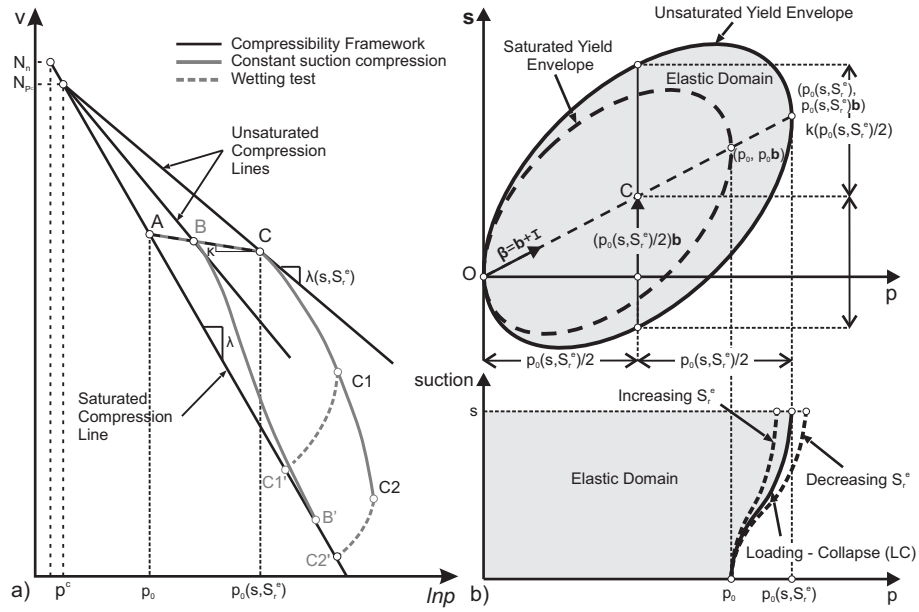

FIGURE 2 a) The proposed unsaturated compressibility framework and; b) The complete Yield Envelope in the stress - partial saturation hyperspace

2.3 | Flow Rule

Following the assumption that during anisotropic consolidation the PYE aligns with the consolidation stress path, the CMUA model incorporates a non associated flow rule, necessary to predict realistic plastic dilation. This is a quite common assumption for anisotropic models (i.e, [28, 15]), while recently Dafalias and Taiebat [16] claimed that the added versatility of a non associated flow rule proves beneficial for undrained loading simulation. However, it should be mentioned that alternative options exist. For instance, if the hardening rule bounds the yield surface rotation to inclinations lower than the consolidation obliquity (i.e, [44]), an anisotropic model can still be accompanied by an associated flow rule without significantly sacrificing plastic dilation predictions.

The CMUA flow rule is based on a Plastic Potential Surface (PPS), as depicted in figure 3. The flow rule determines the plastic strain increment $\dot{\boldsymbol{\varepsilon}}^p$, through an incrementally linear relation:

$$\dot{\boldsymbol{\varepsilon}}^p = \dot{\lambda}\boldsymbol{P} \tag{19}$$

where $\dot{\lambda}$ the plastic multiplier computed as:

$$\dot{\lambda} = \frac{1}{H}\left(\boldsymbol{Q} : \dot{\boldsymbol{\sigma}} + \frac{\partial f}{\partial s}\dot{s} + \frac{\partial f}{\partial S_r^e}\dot{S}_r^e\right) \tag{20}$$

The plastic modulus H is calculated by employing the consistency condition on a later stage, tensor $\boldsymbol{Q} = (Q, \boldsymbol{Q}') = \left(\frac{\partial f}{\partial p}, \frac{\partial f}{\partial \boldsymbol{s}} - \frac{1}{3}\left(\frac{\partial f}{\partial \boldsymbol{s}} : \boldsymbol{I}\right)\boldsymbol{I}\right)$ while the plastic potential tensor $\boldsymbol{P}$ is calculated using the normality rule ($\boldsymbol{P} = (P, \boldsymbol{P}') =$

$\left(\frac{\partial g}{\partial p}, \frac{\partial g}{\partial \boldsymbol{s}} - \frac{1}{3}\left(\frac{\partial g}{\partial \boldsymbol{s}} : \boldsymbol{I}\right)\boldsymbol{I}\right)$) on the following PPS:

$$g(p, \boldsymbol{s}, \theta, \boldsymbol{d}) = \frac{1}{c^2}(\boldsymbol{s} - p\boldsymbol{d}) : (\boldsymbol{s} - p\boldsymbol{d}) - p(\theta - p) \tag{21}$$

In equation 21, θ is the size of the PPS, $\boldsymbol{d}$ is a tensor controlling the orientation of the PPS in all deviatoric planes and c a material constant defining the ratio of the axes of the proposed ellipsoid and further associated with the slope of the critical state line in the generalized stress space ($c = \sqrt{2/3}M$).

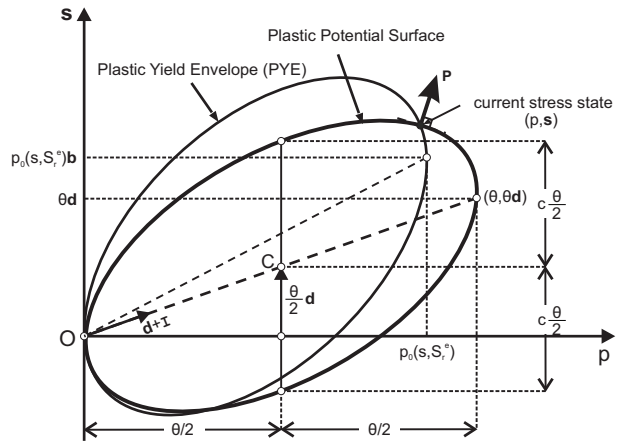

FIGURE 3 The model's flow rule

Regarding the PPS orientation tensor $\boldsymbol{d}$, it is assumed to follow a linear relation with its yield surface counterpart $\boldsymbol{b}$, through parameter χ according to:

$$\boldsymbol{d} = \chi \boldsymbol{b} \tag{22}$$

Parameter χ controls the relative orientation between PYE and PPS. It is calibrated to reproduce the desired dilatancy, under any given stress path, following the procedure described in Appendix A. The size of the plastic potential function θ is calculated to ensure that the PPS satisfies any given plastic state ($g(p, \boldsymbol{s}) = 0$) according to:

$$\theta = p + \frac{\frac{1}{c^2}(\boldsymbol{s} - p\boldsymbol{d}) : (\boldsymbol{s} - p\boldsymbol{d})}{p} \tag{23}$$

2.4 | Hardening Rule

For the evolution of the hardening variables (p_0 & $\boldsymbol{b}$), the CMUA model employs a mixed hardening rule consisting of an isotropic component for the evolution of the size of the distorted ellipsoid under saturated conditions (represented through p_0) and a kinematic component to control the distortion of the SatYE through the anisotropy tensor $\boldsymbol{b}$.

2.4.1 | Isotropic Hardening

The isotropic part of the rule is derived upon the desirable compressibility behaviour and its evolution with anisotropy. In section 2.2.1, the size of the SatYE was correlated with the size of the intrinsic isotropic envelope (p_0^*) and with anisotropy tensor $\boldsymbol{b}$, concluding to equations 12 and 13. The incremental form of the isotropic hardening rule is now calculated by differentiating equation 12:

$$\dot{p_0} = A\dot{p_0^*} + \dot{A}p_0^* \tag{24}$$

where for the increment of quantity A we calculate:

$$\dot{A} = \frac{2A \cdot r_s}{(\kappa - \lambda)} \frac{(N_\eta - \Gamma)}{\left(1 - \frac{1}{c^2}\boldsymbol{b} : \boldsymbol{b}\right)} \frac{1}{c^2}\boldsymbol{b} : \dot{\boldsymbol{b}} \tag{25}$$

To describe the evolution of the size of the intrinsic isotropic envelope ($\dot{p_0^*}$) we adopt the MCC hardening rule:

$$\dot{p_0^*} = \frac{v}{\lambda - \kappa} p_0^* \dot{\varepsilon_v^p} = \frac{v}{\lambda - \kappa} p_0^* \dot{\lambda} P \tag{26}$$

while p_0^* follows equation 9. The proposed isotropic hardening rule is downwards compatible with the MCC hardening rule, as whenever an isotropic material state is examined, $\boldsymbol{b} : \boldsymbol{b} = 0$ and thus, $p_0 = p_0^*$ and $\dot{p_0} = \dot{p_0^*}$, causing equation 26 to reduce to the MCC hardening. On the other hand, for anisotropically consolidated soil elements, the size of the yield surface follows its orientation through the anisotropy tensor $\boldsymbol{b}$, with the reproduced behaviour being in line with the proposed compressibility framework through parameter r_s in equation 13.

2.4.2 | Kinematic Hardening

The kinematic hardening rule describes the evolution of the soil's memory of preferred directions or in other words its memory of anisotropy. The proposed model postulates directly on the incremental form of the anisotropy tensor $\boldsymbol{b}$ and consists of two subcomponents with an additive effect:

$$\dot{\boldsymbol{b}} = \dot{\boldsymbol{b}_o} + \dot{\boldsymbol{b}_d} \tag{27}$$

The first part $\dot{\boldsymbol{b_o}}$ takes the following form:

$$\dot{\boldsymbol{b}_o} = \frac{1}{p_0(s, S_r^e)} \psi_v^p (\boldsymbol{s} - p\boldsymbol{b}) \dot{\varepsilon_v^p} \tag{28}$$

This subcomponent is similar to the hardening rule of the Kavvadas [28] MIT-E1 constitutive model. It is responsible for rotating the SatYE axis towards the direction of the imposed stress path. The magnitude of anisotropy change is assumed proportional to the plastic volumetric strain increment $\dot{\varepsilon_v^p}$, while $(\boldsymbol{s} - p\boldsymbol{b})$ is a stress attractor dragging the SatYE axis towards the direction of the imposed stress path. Parameter ψ_v^p controls the rate of evolution, while the size of the yield surface $(p_0(s, S_r^e))$ is used for dimensioning.

The second part $\dot{\boldsymbol{b_d}}$ is based on an idea initially discussed by Wheeler [43] and further exploited by the authors [39]. It can accommodate in a unified and natural way the strain softening behaviour exhibited by anisotropically consoli-

dated soil samples when subjected to triaxial undrained loading together with unique critical state conditions irrespective of the initial anisotropy and of the stress path followed. The main idea is that the aforementioned behaviour is the outcome of an anisotropy degradation mechanism. In more detail, it is suggested that the plastic straining occurring during any stress path which can lead to failure (e.g., triaxial undrained loading), produces a progressive loss in the material's memory of anisotropy. In terms of constitutive modelling this can be described as a progressive re-orientation of the yield surface towards the isotropic axis, with a common critical state associated with an isotropic yield surface. The following expression is proposed to describe the anisotropy degradation mechanism:

$$\dot{\boldsymbol{b}}_d = -\frac{1}{[p_0(s, S_r^e)]^2}\boldsymbol{b}\,(\boldsymbol{s}-p\boldsymbol{b}) : (\boldsymbol{s}-p\boldsymbol{b})\,\zeta_q^p\dot{\varepsilon}_q^p \tag{29}$$

The de-orientation is proportional to the increment of the magnitude of the plastic deviatoric strain $\dot{\varepsilon}_q^p$, calculated as $\dot{\varepsilon}_q^p = \sqrt{\frac{2}{3}\left(\dot{\boldsymbol{e}}_p : \dot{\boldsymbol{e}}_p\right)}$. Parameter ζ_q^p controls the intensity of the distortion while the size of the yield surface is used for dimensioning. Equation 29 includes the anisotropy tensor as an attractor, to drag the yield surface towards the isotropic axis and to freeze the rotation when the yield surface becomes isotropic ($\boldsymbol{b} = \boldsymbol{0}$). It additionally includes the term $(\boldsymbol{s}-p\boldsymbol{b}) : (\boldsymbol{s}-p\boldsymbol{b})$ to ensure that during radial stress paths the first part ($\dot{\boldsymbol{b}}_{\boldsymbol{o}}$) becomes dominant. It is evident that the proposed rule assumes that critical state conditions are described through an isotropic ellipse irrespective of the initial level of anisotropy. The proposed assumption, apart from compatible with the MCC model, additionally eliminates the necessity to somehow determine the inclination of the yield surface at critical state. However, we should mention that the critical state of anisotropically consolidated soil elements is still a hot research issue [16, 17] mainly due to the lack of conclusive experimental evidence.

The assumed isotropic yield surface at critical state further implies that some of the model's parameters are correlated. It can be calculated that the model will predict a Γ value (location of the CSL) equal to $\Gamma = N_{iso} - (\lambda-\kappa)\ln(1+\frac{c^2}{k^2})$. This relationship is derived in the triaxial stress space (p, $q = \sqrt{(3/2)(\boldsymbol{s} : \boldsymbol{s})}$) and holds true for the simplest case where c, k are assumed independent of the examined deviatoric plane. Through the aforementioned equation parameter k can be used to control the spacing between the ICC (N_{iso}) and the CSL (Γ) in the $v - \ln p$ plane.

Finally, the consistency condition is applied to plastic states lying on the yield surface, which ensures that during plastic loading the material state remains on the yield surface:

$$\dot{f} = 0 \Rightarrow \dot{f} = \boldsymbol{Q} : \dot{\boldsymbol{\sigma}} + \frac{\partial f}{\partial s}\dot{s} + \frac{\partial f}{\partial S_r^e}\dot{S}_r^e + \frac{\partial f}{\partial p_0}\dot{p_0} + \frac{\partial f}{\partial \boldsymbol{b}} : \dot{\boldsymbol{b}} = 0 \tag{30}$$

Applying it to equation 18 and combining with equation 20 we may calculate the Plastic Modulus H:

$$H = -\left(\frac{\partial f}{\partial p_0}\overline{p_0} + \frac{\partial f}{\partial \boldsymbol{b}} : \overline{\boldsymbol{b}}\right) \tag{31}$$

where the hardening variables increments ($\dot{p_0}$ & $\dot{\boldsymbol{b}}$) have been expressed as $\dot{p_0} = \dot{\lambda}\overline{p_0}$ and $\dot{\boldsymbol{b}} = \dot{\lambda}\overline{b}$.

3 | MODEL EVALUATION

This section evaluates the capabilities of the CMUA model by simulating a series of typical stress paths under both saturated and unsaturated conditions. The simulation has been realized in a single material point utilizing a suitable computer code developed in Fortran. For simulations under unsaturated conditions, the model is coupled with the

TABLE 1 Parameters used in the presented analyses

Saturated mechanical model parameters							
κ	0.01	k	0.93897	N_{iso}	2.10	ψ_v^p	40, 100
λ	0.07	c	0.93897[*1]	r_s	0.75	ζ_q^p	120, 400
ν	1/3	χ	0.469[*2]				
Unsaturated mechanical model parameters				WRM Parameters			
r	0.8	γ	0.8	ϕ	0.011	m	0.567
$\beta(kPa^{-1})$	100.0	$p^c(kPa)$	1 kPa	n	1.005	ψ	4.0
				α	2.5		

[*1] is equivalent to $M = 1.15$; [*2] calibrated for $K_0 = 0.55$.

void ratio dependent Water Retention Model (WRM) of Gallipoli et al. [21], where degree of saturation equals:

$$S_r = \frac{1}{\left[1 + \left((\phi(v-1)^{\psi})\, s\right)^n\right]^m} \tag{32}$$

In equation 32, ϕ, ψ, n, m are material constants and v the specific volume.

The simulation uses a set of material parameters which represent a typical silty soil. Table 1 summarizes the adopted material constants, including the WRM's parameters. The presented work additionally includes a limited parametrical investigation of the effect that different values of the hardening rule parameters ψ_v^p and ζ_q^p have on the reproduced mechanical behaviour. It facilitates an easier calibration of the proposed model to experimental results, where selection of these parameters necessitates trial and error simulations.

Figure 4 presents and compares two anisotropic consolidation tests under saturated conditions; a K_0 radial stress path and an oedometric compression test (1D). Both tests are applied to an isotropically consolidated material element ($\boldsymbol{b} = \mathbf{0}$, $p_0 = 100kPa$) and include an evolving anisotropy. The $1D$ compression test originates from a normally consolidated material state ($p = 100kPa$, $q = 0kPa$), while the K_0 test requires unloading and adjustment of the initial stress state to the required obliquity $\eta = 0.6428$ ($p = 60kPa$, $q = 38.565kPa$), in line with the assumed $K_0 = 0.55$.

Figure 4a reveals that on the $p - q$ plane, the stress path of the $1D$ compression test aligns with the stress path of the K_0 test, reflecting the successful calibration of the flow rule and the model's ability to reproduce the desired K_0 value. Moreover at the end of compression, the yield surface is oriented to the stress path of the consolidation, indicating that the material has developed the corresponding "memory" of induced anisotropy. This is also reflected in the compression curves of figure 4b, where both tests lie on the K_0-intrinsic compression curve as described by the ICF underlying the model's hardening rule. Figure 4b further illustrates the effect of parameter ψ_v^p. Note that the smaller value ($\psi_v^p = 40$) delays the adjustment of the compressibility behaviour to the desired compression curve compared to the $\psi_v^p = 100$ case, reflecting the slower adjustment of anisotropy to the imposed stress obliquity.

Figure 5 plots results from undrained triaxial compression and extension tests on saturated samples. They cor-

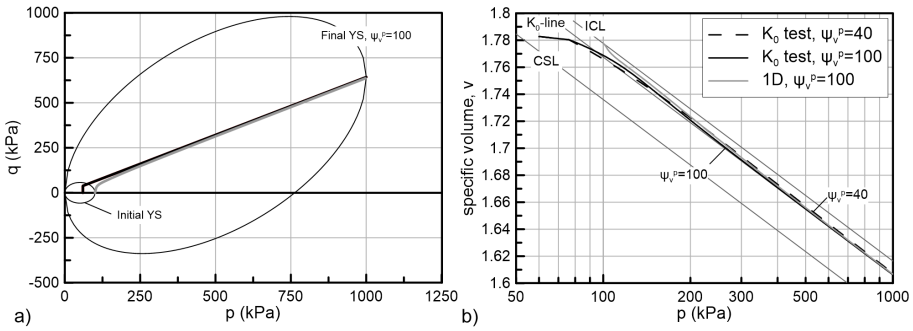

FIGURE 4 Comparison between radial and $1D$ compression

respond to two different initial anisotropic normally consolidated stress states at $\eta_i = 0.6425$ and $\eta_i = 0.25$, with $p = p_0 = 200kPa$. In graph 5b, the stress-strain curves clearly depict the strain-softening behaviour accompanying the undrained compression tests and how parameter ζ_q^p controls the rate of strength degradation towards critical state. Following the assumptions of the proposed model's hardening rule, critical state is reached when the material eliminates any evidence of its anisotropic background. This is reflected in graph 5d which plots the gradual anisotropy degradation ($b_q = \sqrt{(3/2)\boldsymbol{b} : \boldsymbol{b}}$) with the onset of plastic deviatoric strains resulting to an isotropic yield surface at critical state, the latter also depicted in graph 5a (only the $\zeta_q^p = 400$ tests reach critical state).

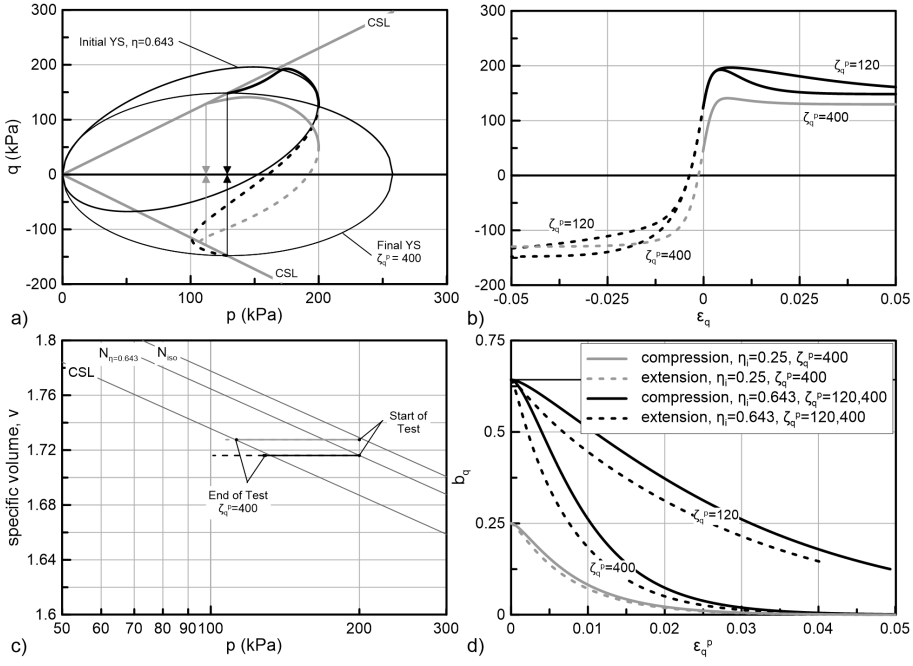

FIGURE 5 Undrained triaxial compression on anisotropically consolidated soil elements

We may further observe the advantages of this common "isotropic" critical state. In graph 5a, the soil elements

loaded from the same initial anisotropic stress state, end up to a unique critical state, as depicted by the vertical arrows which denote a common isotropic stress (p) at critical state, irrespective of whether compression or extension is examined. Dafalias and Taiebat [16] discuss the significance of such a uniqueness of critical state, additionally emphasizing on the inability of most of the existing anisotropic constitutive models to capture such a behaviour. For extension tests this anisotropy degradation mechanism towards a unique critical state produces a hook type behaviour, in line with common laboratory observations (e.g., Gens [22]). Moreover, in the $v - \ln p$ plane, the results suggest a common and well defined critical state line for soil elements with different initial anisotropic background, illustrating that the proposed model's critical state is independent of the initial anisotropy.

Figure 6 extends the discussion to the unsaturated features of the CMUA model by presenting the results of a series of isotropic compression tests under different constant suction levels. All stress paths initiate from an isotropic, saturated (zero suction), overconsolidated material state ($p = \overline{p} = 50kPa$, $p_0 = 100kPa$) and are progressively dried under constant net (total) stress to various suction levels ranging from $s = 50kPa$ to $s = 5MPa$, thus covering an extended portion of the assumed water retention curve (see graph 6b). Following drying, the simulation involves isotropic compression under constant suction up to a net stress level equal to $\overline{p} = 5MPa$.

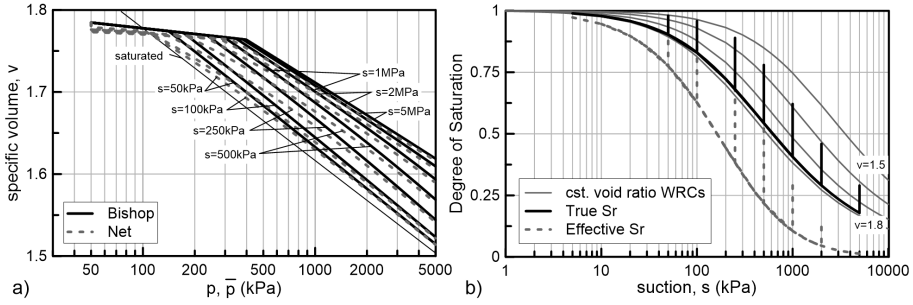

FIGURE 6 Isotropic compression under different suction levels

Inspection of figure 6a shows that the model predicts a non-linear increase in apparent preconsolidation pressure with increasing suction, while the elastic compressibility is represented by a common swelling curve when plotted in terms of Bishop's stress and by suction dependant swelling curves when plotted in terms of net stress. This is the natural outcome of Bishop's stress formulation as the latter has been extensively discussed by Jommi [25]. Upon yielding, the compression curves exhibit an initial post yield compressibility which appears to reduce as the suction level increases (more profound in the net stress curves), while further compression results to a gradually increasing compressibility as a result of the increasing degree of saturation predicted by the adopted water retention model.

Figure 7a reveals the significance of such an evolving compressibility in the predicted volumetric deformation upon wetting. It summarizes the results of a series of wetting tests under different constant net stress levels and different initial suction levels. In fact these wetting tests initiate from various points on the compression curves presented in figure 6a. They are simulated by gradually reducing suction to zero while maintaining a constant net stress. The obtained curves of accumulated volumetric strains during wetting reveal that the model can reproduce the dependance of the net volumetric behaviour (swelling vs collapse) on the level of confinement, an increasing collapse potential as the initial level of suction increases and also a varying collapse potential with net stress, which leads to a maximum of collapse. The reproduced behaviour is in line with typical experimental results [32].

Figure 7b evaluates the model's shear strength predictions under unsaturated conditions. It plots normalized shear strength results from a series of constant suction triaxial shear tests, under three different levels of confinement.

Results are for initially isotropically consolidated material states ($p = p_0 = 100kPa$), dried to the desired suction level, compressed to the relevant confinement pressure and subsequently sheared to failure. The vertical axis corresponds to the ratio of the peak deviatoric stress exhibited during loading over its counterpart under zero suction. The results illustrate the advantage of Bishop's stress implementation in reproducing naturally a nonlinear evolution of shear strength with suction and also the diminishing beneficial effect of suction in increasing shear strength as the level of confinement increases.

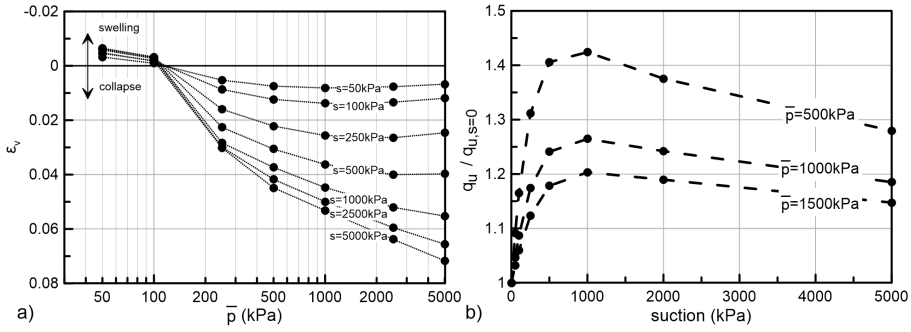

FIGURE 7 a) Volumetric behaviour upon wetting for different net stress and suction levels and; b) Evolution of peak deviatoric stress with suction

At this point, it is also interesting to extend the discussion to the combined effects of partial saturation and anisotropy and how these are reflected in the model's predictions. In that respect, figure 8a compares the compression lines, plotted in terms of net stress, between isotropically and anisotropically (1D) consolidated soil elements, under four different suction levels. All tests initiate from the same isotropic state ($p = 50kPa$, $p_0 = 100kPa$,$\boldsymbol{b} = \mathbf{0}$). Suction is increased to the desired level under constant net stress to simulate drying and afterwards compression under isotropic and one-dimensional conditions is imposed. The results reflect the combined effect of both anisotropy and partial saturation as these have been separately discussed previously. In both cases, the apparent presconsolidation pressure increases with suction while the post yield compressibility is non-linear. When compared at the same suction level, the $1D$ compression curves plot to the left of their isotropic counterparts, following the compressibility framework adopted in the proposed model and reflecting the beneficial effect that anisotropic consolidation has on reducing the void ratio during compression, in line with common experimental observations [1].

Figure 8b presents the evolution of the computed coefficient of earth pressure at rest with suction, expressed in terms of net stress ($\overline{K_0} = \overline{\sigma_h}/\overline{\sigma_v}$), for different levels of vertical net stress. The results indicate that partial saturation leads to a decrease in the $\overline{K_0}$ with respect to the assumed saturated value ($K_0 = 0.55$). In terms of constitutive modelling the reduced K_0 with partial saturation is a consequence of Bishop's stress implementation. In more detail, the flow rule is calibrated under saturated conditions to reproduce the desired K_0 value, equal to 0.55 in the examined case. It is evident that in terms of Bishop's average skeleton stress the same K_0 value will apply irrespective of the state of partial saturation. On the other hand, any unsaturated, non-isotropic stress path exhibits a higher obliquity in terms of net stress with respect to its Bishop's stress counterpart ($q/\bar{p} > q/p$). We may calculate that for any given saturated K_0 value the proposed model under stabilized anisotropic conditions will predict a $\overline{K_0}$ value equal to:

$$\overline{K_0} = K_0 - (1 - K_0) \cdot \frac{s \cdot S_r^e}{\overline{\sigma_v}} \tag{33}$$

The variation of $\overline{K_0}$ value with partial saturation and vertical net stress as predicted through equation 33 is plotted in figure 8b.

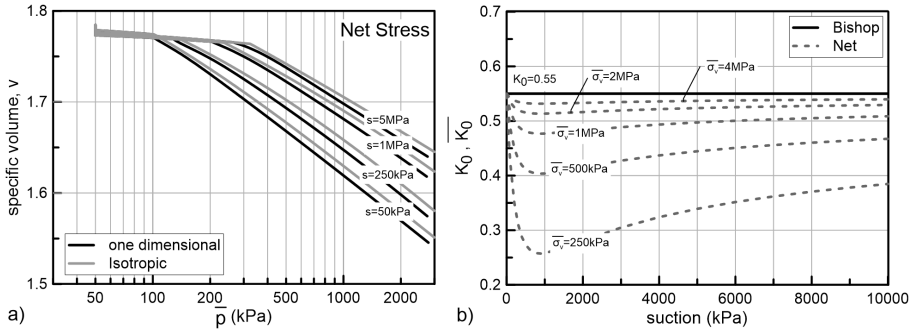

FIGURE 8 a) Constant suction isotropic and $1D$ compression; b) variation of coefficient of earth pressure at rest with suction

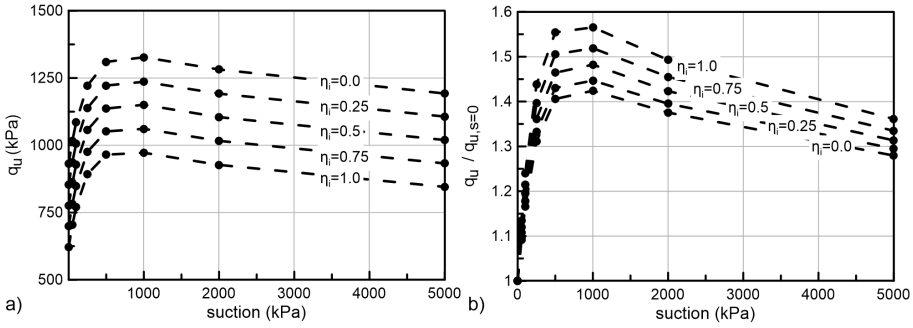

FIGURE 9 Evolution of peak deviatoric strength with partial saturation and anisotropy

Finally, figure 9 evaluates the combined effect of partial saturation and anisotropy in shear strength predictions. It summarizes the exhibited peak strength values from a series of constant suction triaxial compression tests applied on soil elements initially consolidated to different stress obliquities (η_i) under saturated conditions up to $p = p_0 = 500kPa$. After drying to the desired suction level drained (constant suction) triaxial compression is applied under a constant confinement ($\overline{p} = 500kPa$). The exhibited peak strength values indicate that an increase in the initial anisotropy leads to a reduced ultimate deviatoric stress, irrespective of the level of the applied suction. This is in accordance with the usually observed experimental behaviour (e.g., Gens [22]) even under saturated conditions and is attributed to the increasing proximity of the initial stress state to the critical state line with increasing anisotropy, resulting to failure under a lower $\overline{p}$ as anisotropy increases. With respect to the evolution of shear strength with suction, under a given initial anisotropy, this follows the same trend with isotropically consolidated soil elements as previously discussed (see figure 7). However, in figure 9b it is interesting to notice that when peak strength is normalized with respect to the saturated behaviour ($q_{u,s}/q_{u,s=0}$), it turns out that the effect of partial saturation in increasing soil strength gets more profound as initial anisotropy increases. This is also a consequence of the fact that failure occurs under a higher mean stress with decreasing anisotropy; as previously discussed, the higher the net mean stress is, the less efficient partial

TABLE 2 The calibrated model parameters corresponding to the LCT behaviour

Saturated model parameters							
κ	0.008	k	0.79046	N_{iso}	1.7950	ψ_v^p	60
λ	0.067	c	0.91287	r_s	0.47	ζ_q^p	160
ν	1/3	χ	0.49444				

saturation becomes in increasing shear strength.

4 | COMPARISON WITH EXPERIMENTAL MEASUREMENTS

This section extends evaluation of the CMUA model through a calibration against available experimental results from the international literature. It evaluates: a) the anisotropic capabilities of the proposed model under saturated conditions against the Lower Cromer Till (LCT) experimental investigation offered by Gens [22] and; b) the combined effect of anisotropy and partial saturation against the Jossigny Silt experimental investigation of Casini [12].

4.1 | The Lower Cromer Till

Gens [22] investigated the anisotropic behaviour of LCT, a glacial till of low plasticity, which according to the Unified Soils Classification System (USCS) is characterized as a Clayey Sand (SC). The available experimental results concentrate on saturated conditions and include a large number of consolidation tests under different stress paths and boundary conditions as well as triaxial tests on both isotropically and anisotropically consolidated soils. The model was calibrated against the consolidation stage and subsequent undrained triaxial compression of an isotropically and a K_0 consolidated sample. Then, it was applied to consolidation stress paths under different stress obliquities and to subsequent drained and undrained triaxial tests. Table 2 summarizes the parameters derived during calibration. They are used in the simulation exercise presented in figures 10 & 11.

In more detail, figure 10 compares the model's predictions during anisotropic consolidation with the available experimental behaviour. Fig. 10a regards two K_0 radial consolidation stress paths, while the presented simulation follows the complete sample preparation and consolidation procedure, namely an initial $1D$ compression in a large oedometer up to $\sigma_v = 200kPa$, followed by unloading and subsequent testing under K_0 conditions in a triaxial cell up to $p = 500kPa$. We observe that the model provides an accurate description of the experimentally observed behaviour, reflecting the successful calibration of the model's compressibility parameters. Figure 10b evaluates the model's ability to describe the dependance of virgin compression lines on the level of induced anisotropy during consolidation. The experimental results concern initially isotropic specimens, which are consolidated in a triaxial cell to different stress obliquities up to $p = 233kPa$. Note that these experimental results have not been used during calibration but instead the compressibility framework was calibrated against an isotropic consolidation to define N_{iso}, an oedometer test to define N_{K_0} and also based on the Γ value identified by the two triaxial tests examined. Nevertheless, the predicted compression curves in the $v - \ln p$ plane match very well the experimental results, demonstrating that the adopted

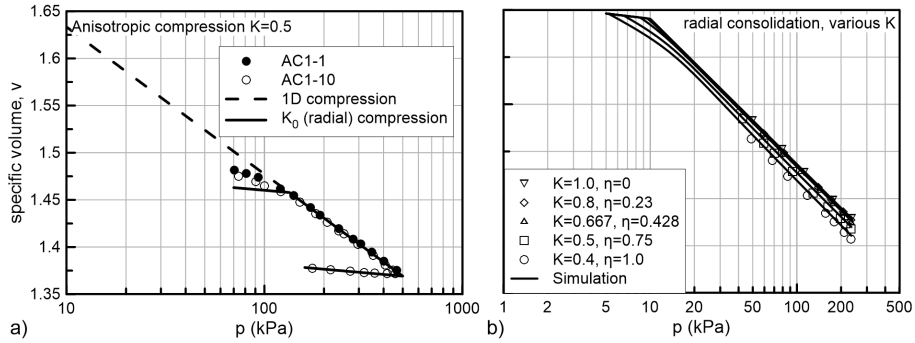

FIGURE 10 a) 1D and K_0 consolidation; b) radial consolidation under various K for the LCT [22]

ICF [8] and its integration in the hardening rule of the CMUA model can successfully represent the spacing between compression curves produced by consolidation at different stress ratios.

With the final state of the previously discussed compression tests serving as an initial state, drained and undrained triaxial compression tests were simulated. They revealed that the model severely overpredicts the peak strength during undrained compression, unless an initial inclination of the yield surface which is decreased by almost 60% ($b_q = 0.4 \cdot \eta$) with respect to the obliquity of the consolidation path is assumed. Following the assumption of a reduced initial yield surface inclination, figure 11 presents the simulation results and compares them with the corresponding experimental data. We may observe that the model provides a fair representation of the LCT behaviour, especially for the specimen sheared after a K_0 consolidation which has been used during calibration. The model predicts well the ultimate, critical state conditions irrespective of the initial level of anisotropy, a strong indication towards the validity of the model's hardening rule assumption that critical state corresponds to an isotropic yield surface. Moreover in figures 11b & d we may observe that during drained compression, the model predicts very well the continuously strain hardening response and the reducing potential for contraction, with increasing initial anisotropy, despite the fact that these results have not been used during calibration.

It should be emphasised though that the discussed simulation exercise does not confirm the model's hypothesis that the initial position of the yield surface is aligned with the stress path of the consolidation. Given that the LCT results correspond to stabilized anisotropic fabric prior to shearing, the only alternative is to reexamine the working hypothesis of the MIT-E1 model also adopted in this model. It is possible that the aforementioned hypothesis is more realistic for clays and that silty or sandy soils do not develop such a strong anisotropic fabric.

4.2 | The Jossigny Silt

Casini [12] performed a series of experiments to access the unsaturated behaviour of the Jossigny Silt (JS). JS is a Silty Clay of low plasticity (ML) according to the USCS. For specimen preparation, the researcher used static compaction under 1D conditions to prepare initially unsaturated specimens with a water content equal to 13% and a dry unit weight of $14.5kN/m^3$. Then a series of radial compression tests under different stress obliquities, constant suction triaxial compression tests and constant suction oedometer tests were performed. The axis translation technique was used for testing under different suction levels. Table 3 reports the model's parameters derived during calibration. The reported water retention parameters correspond to the Gallipoli et al. (2003) WRM (see eq. 32) and for the initial hardening variables $p_0^* = 40kPa$ and $b_q = 0.15$ are selected, the latter reflecting the anisotropic sample preparation

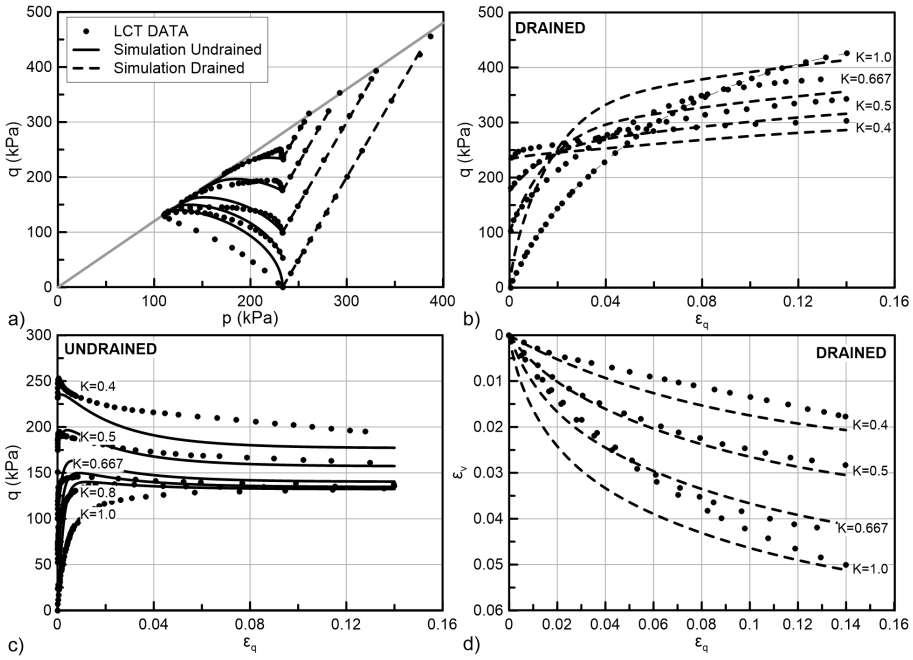

FIGURE 11 Drained and undrained triaxial compression under different initial anisotropy for the LCT [22]

(1*D* compaction).

Figure 12 compares the model's predictions with available experimental results from constant suction oedometric compression tests. The initial void ratio has not been fine tuned to the experimental data but is the outcome of the compressibility framework, initially calibrated on a set of saturated tests reported also in Casini (2008). The model proves capable of describing the dependance on suction and also the evolving compressibility under constant suction compression. This is attributed to the incorporated compressibility framework and its double dependance on suction and degree of saturation. Note that in figure 12b, which depicts the accompanying water retention behaviour, the experimental data exhibit a significant variation of degree of saturation during compression under constant suction. It should be noted that a contributing factor to the successful simulation is the Gallipoli et al. [21] WRM adopted, which proves capable of capturing the dependance of the water retention properties on void ratio.

Figure 13 presents triaxial compression tests under constant suction ($s = 200kPa$) and the complete stress paths (initial consolidation and subsequent shearing) are simulated. During simulation, the stress path is prescribed in terms of net stress, while the presented comparison in terms of Bishop's stress concerns: a) computed stress path based on the WRM's predictions and; b) the experimentally measured stress path. The fact that in figure 13a simulated and experimental Bishop's stress paths coincide reflects the successful calibration of the WRM and is a prerequisite for accurate shear strength predictions for any Bishop's stress model. Figure 13 confirms that the model provides successful predictions of the exhibited stress strain relation. Additionally it captures very satisfactory the contractant behaviour of the anisotropically consolidated TRX06 and TRX07 specimens which are sheared at the "wet of critical". On the other hand, at least with the selected calibration, the model underestimates the dilative response of the isotropically consolidated specimens TRX01 and TRX02 as it seems that they were sheared under a higher overconsolidation ratio compared to the one that the CMUA predicts. However, the model captures the trend towards a reducing contrac-

TABLE 3 The calibrated model parameters corresponding to the Josigny Silt behaviour

Saturated mechanical model parameters							
κ	0.006	k	1.0206	N_{iso}	2.25	ψ_v^p	40
λ	0.11	c	1.0206	r_s	2.0	ζ_q^p	80
ν	1/3	χ	0.4945				
Unsaturated mechanical model parameters				**WRM Parameters**			
r	0.4	γ	1.0	ϕ	1.318	m	0.15
$\beta(MPa^{-1})$	30.0	$p^c(kPa)$	6 kPa	n	1.34	ψ	6.04
				α	1.5		

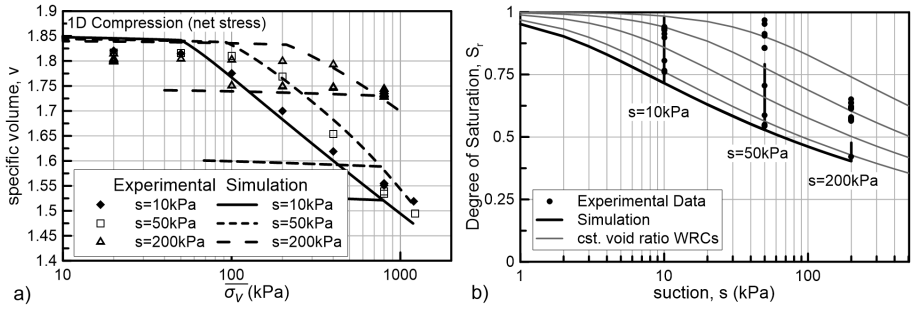

FIGURE 12 1D consolidation under three different constant suction levels for the JS [12]

tion with a reducing stress path obliquity and an increasing overconsolidation ratio. The same comments apply for the behaviour in the $v - \ln \overline{p}$ plane, depicted in figure 13c.

5 | CONCLUSIONS

The paper presents and evaluates a critical state constitutive model for anisotropically consolidated, unsaturated, non-expansive soils (CMUA). The model enhances the flow and hardening rules of the MIT-E1 anisotropic constitutive model. Then it takes advantage of Bishop's average skeleton to extend it into the unsaturated regime, favoring numerical implementation and the unified analyses of anisotropic, saturated and unsaturated material states. The proposed model includes a distorted ellipsoid as its yield surface, a non - associated flow rule which can be easily calibrated to reproduce realistic K_0 values and a mixed hardening rule. The yield envelope in the stress - suction hyperspace is completed by a Loading - Collapse surface based on an unsaturated compressibility framework with a double dependence on both suction and on the macrostructural degree of saturation.

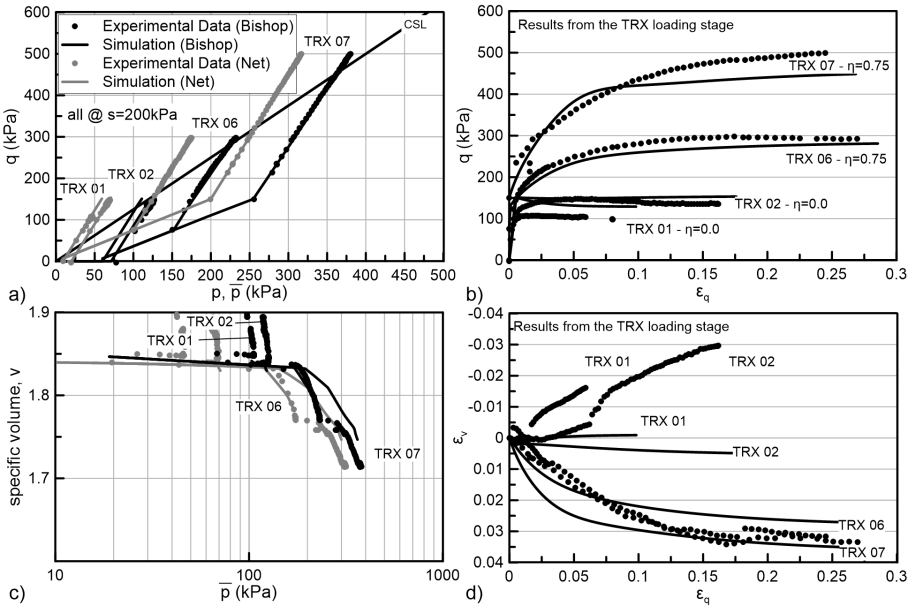

FIGURE 13 Constant suction ($s = 200kPa$) triaxial compression tests under different anisotropic conditions for the JS [12]

The mechanical part of the model employs fourteen (14) material parameters. Five (5) of them are the well known MCC parameters (κ, λ, c, ν, N_{iso}) while another five (5) complete the anisotropic saturated base of the model (χ, k, r_s, ψ_v^p, ζ_q^p). The CMUA model requires an increased number of parameters compared to other popular anisotropic models (i.e., [44]) but this is the price one has to pay for increased flexibility in matching experimental results. The unsaturated part of the model requires another four mechanical parameters to control the unsaturated compressibility and the LC surface (r, β, ,γ, p^c). The model's anisotropic and unsaturated capabilities can be deployed separately or in parallel. The vast majority of the employed parameters are the outcome of a straight forward calibration on the results of common geotechnical laboratory tests with only two (ψ_v^p, ζ_q^p) requiring trial and error simulations for fine tuning. Moreover, as with any Bishop's stress constitutive model, activation of the unsaturated features of the model requires additional parameters for the WRM. In its current version the model has been linked to the Gallipoli void ratio dependent WRM which necessitates another four parameters (ϕ, n, m, ψ) while finally parameter α is also required to scale degree of saturation for macro-structure, increasing the total number of parameters to nineteen (19).

Numerical evaluation of the proposed model confirms that the model is capable of reproducing: a) the dependence of compression curves on the level of stress obliquity; b) strain - softening for anisotropically consolidated soil elements subjected to undrained compression; c) unique critical state conditions independent of the initial anisotropy and of the stress path followed. Both points (b) and (c) are the outcome of the incorporated deviatoric part of the hardening rule which with the onset of plastic deviatoric strains reduces the yield surface inclination towards the isotropic axis to account for a progressive elimination of the soil's memory of anisotropy. In the unsaturated domain, the CMUA model captures: a) a non-linear increase in the shear strength with suction following the evolution of Bishop's average skeleton stress; b) a non-linear increase in the apparent preconsolidation pressure with suction; c) an evolving post yield compressibility even for compression under constant suction and; d) a maximum of collapse during wetting as a

consequence of the aforementioned evolving compressibility.

A preliminary validation of the model against experimental results proved that the model is capable of producing fair simulations of the experimentally observed behaviour. However, it also revealed shortcomings of the proposed formulation and especially regarding the first part of the hardening rule and the assumed orientation of the yield surface during anisotropic compression. Moreover, in its present state, the model is more suitable for simulations of normally and slightly over-consolidated material states as it includes a relative increased elastic domain, which can potentially hinder its simulation capabilities at the “dry side" of the critical state. Thus, future versions of the CMUA model need to elaborate the formulation (i.e., updated hardening, bounding surface plasticity) and to further validate its simulation capacity against additional experimental results with more emphasis on the combination of anisotropy and partial saturation.

references

[1] Al-Sharrad MA, Gallipoli D, Wheeler SJ. Experimental investigation of evolving anisotropy in unsaturated soils. Géotechnique 2017;Ahead of Print(0):1–17.

[2] Al-Sharrad MA, Gallipoli D. Incorporating anisotropy in the Barcelona basic model. E3S Web Conf 2016;9:17003.

[3] Alonso EE, Pereira JM, Vaunat J, Olivella S. A microstructurally based effective stress for unsaturated soils. Géotechnique 2010;60(12):913–925.

[4] Alonso EE, Gens A, Josa A. A constitutive model for partially saturated soils. Géotechnique 1990;40(3):405–430.

[5] Alonso EE, Pinyol NM, Gens A. Compacted soil behaviour: initial state, structure and constitutive modelling. Geotechnique 2012;63(6):463–478.

[6] Alonso E, Pinyol N, Gens A. Compacted soil behaviour: initial state, structure and constitutive modelling. Géotechnique 2013;63(6):463.

[7] Bardanis M, Kavvadas M. Modifying the Barcelona Basic Model to account for residual void ratio and subsequent decrease of shear strength relative to suction. In: Advances in Geo-Engineering - Proceedings of the 1st European Conference on Unsaturated Soils, Durham, UK; 2008. p. 589–595.

[8] Belokas G, Kavvadas M. An Intrinsic Compressibility Framework for Clayey Soils. Geotechnical and Geological Engineering 2011;29(5):855–871.

[9] Bishop AW. The principles of effective stress. Teknick Ukeblad, 39 : 859-863, Norges Geotekniske Institutt; 1959.

[10] Bolzon G, Schrefler B, Zienkiewicz O. Elastoplastic soil constitutive laws generalized to partially saturated states. Géotechnique 1996;46(2):279–289.

[11] Burland J. On the compressibility and shear strength of natural clays. Géotechnique 1990;40(3):329–378.

[12] Casini F. Effecti Del Grado Di Saturazione Sul Comportamento Meccanico Del Limo (in Italian). PhD thesis, La Sapienza University, Rome, Italy; 2008.

[13] Casini F. Deformation induced by wetting: a simple model. Canadian Geotechnical Journal 2012;49(8):954–960.

[14] Cui YJ, Delage P. Yielding and plastic behaviour of an unsaturated compacted silt. Géotechnique 1996;46(2):291–311.

[15] Dafalias YF, Manzari MT, Papadimitriou AG. SANICLAY: simple anisotropic clay plasticity model. International Journal for Numerical and Analytical Methods in Geomechanics 2006;30(12).

[16] Dafalias Y, Taiebat M. Anatomy of rotational hardening in clay plasticity. Géotechnique 2013;63(16):1406–1418.

[17] Dafalias Y, Taiebat M. Rotational hardening with and without anisotropic fabric at critical state. Géotechnique 2014;64(6):507–511.

[18] D'Onza F, Gallipoli D, Wheeler S. Effect of anisotropy on the prediction of unsaturated soil response under triaxial and oedometric conditions 2010;.

[19] Gallipoli D, Bruno AW. A bounding surface compression model with a unified virgin line for saturated and unsaturated soils. Géotechnique 2017;67(8):703–712.

[20] Gallipoli D, Gens A, Sharma R, Vaunat J. An elasto-plastic model for unsaturated soil incorporating the effects of suction and degree of saturation on mechanical behaviour. Géotechnique 2003;53(1):123–135.

[21] Gallipoli D, Wheeler S, Karstunen M. Modelling the variation of degree of saturation in a deformable unsaturated soil. Géotechnique 2003;53(1):105–112.

[22] Gens A. Stress-strain and strength characteristics of a low plasticity clay. PhD thesis, Imperial College London; 1982.

[23] Georgiadis K. Development, implementation and application of partially saturated soil models in finite element analysis. PhD thesis, Imperial College; 2003.

[24] Gonzalez N, Gens A. Evaluation of a constitutive model for unsaturated soils: stress variables and numerical implementation. In: Alonso E, Gens A, editors. Unsaturated Soils - Proc. of the 5th Inter. Conf. on Unsat. Soils, Barcelona, Spain, 6-8 September, 2010 CRC Press/Balkema; 2011. .

[25] Jommi C. Remarks on the constitutive modelling of unsaturated soils. Experimental evidence and theoretical approaches in unsaturated soils 2000;p. 139–153.

[26] Josa A, Balmaceda A, Gens A, Alonso E. An elastoplastic model for partially saturated soils exhibiting a maximum of collapse. In: 3rd international conference on computational plasticity, Barcelona, vol. 1; 1992. p. 815–826.

[27] Karube D, Kawai K. The role of pore water in the mechanical behavior of unsaturated soils. Geotechnical & Geological Engineering 2001;19(3-4):211–241.

[28] Kavvadas M. Non - Linear Consolidation around driven piles in Clays. PhD thesis, Massachussets Institute of Technology (MIT), Cambridge, MA; 1982.

[29] Kavvadas M. General report: Modelling the soil behaviour - Selection of soil parameters. In: Evangelista A, Picarelly L, editors. The Geotec. of hard soils - soft rocks. Proc. of the 2nd Int. Conf. Geotech. Hard Soils-Soft Rocks, Naples, Italy, 12 -14 Oct. 1998, vol. 3; 2000. p. 1441–1481.

[30] Kikumoto M, Kyokawa H, Nakai T, Shahin HM. A simple elasto-plastic model for unsaturated soils and interpretations of collapse and compaction behaviours. vol. 2; 2011. p. 849–855.

[31] Kohgo Y, Nakano M, Miyazaki T. Theoretical aspects of constitutive modelling for unsaturated soils. Soils & Foundations 1993;33(4):49–63.

[32] Lawton EC, Fragaszy RJ, Hardcastle JH. Collapse of compacted clayey sand. Journal of Geotechnical Engineering 1989;115(9):1252–1267.

[33] Leroueil S, Vaughan P. The general and congruent effects of structure in natural soils and weak rocks. Géotechnique 1990;40(3):467–488.

[34] Lewin P, Burland JB. Stress-probe experiments on saturated normally consolidated clay. Géotechnique 1970;20(1):38–56.

[35] Loret B, Khalili N. A three-phase model for unsaturated soils. International Journal for Numerical and Analytical Methods in Geomechanics 2000;24(11):893–927.

[36] Roscoe K, Burland J. On the generalized stress-strain behaviour of wet clay 1968;.

[37] Schofield A, Wroth P. Critical state soil mechanics 1968;.

[38] Sheng D, Fredlund DG, Gens A. A new modelling approach for unsaturated soils using independent stress variables. Canadian Geotechnical Journal 2008;45(4):511–534.

[39] Sitarenios P, Belokas G, Kavvadas M. The Incorporation of new isotropic and kinematic hardening rules in an anisotropic constitutive model. In: Pietruszczak S, Pande GN, editors. Comp. Geomech. - Proc. of the 3rd Inter. Symp. on Comp. Geomech. (ComGeo III), Krakow, Poland, 21-23 Aug., 2013; 2013. p. 85–97.

[40] Sitarenios P, Kavvadas M. A compressibility framework to describe the volume change behaviour of unsaturated clayey soils. Unsaturated Soils: Research & Applications 2014;1:449.

[41] Stropeit K, Wheeler S, Cui Y. An anisotropic elasto-plastic model for unsaturated soils 2008;p. 625–631.

[42] Sun D, Sheng D, Sloan SW. Elastoplastic modelling of hydraulic and stress-strain behaviour of unsaturated soils. Mechanics of Materials 2007;39(3):212–221.

[43] Wheeler S. A rotational hardening elasto-plastic model for clays. In: Proc. of the 14th ICSMFE, Hamburg, vol. 1; 1997. p. 431–434.

[44] Wheeler SJ, Näätänen A, Karstunen M, Lojander M. An anisotropic elastoplastic model for soft clays. Canadian Geotechnical Journal 2003;40(2):403–418.

[45] Wheeler S, Sharma R, Buisson M. Coupling of hydraulic hysteresis and stress–strain behaviour in unsaturated soils. Géotechnique 2003;53(1):41–54.

[46] Whittle AJ, Kavvadas MJ. Formulation of MIT‐E3 Constitutive Model for Overconsolidated Clays. Journal of Geotechnical Engineering 1994;120(1):173–198.

[47] Zhang F, Ikariya T. A new model for unsaturated soil using skeleton stress and degree of saturation as state variables. Soils and Foundations 2011;51(1):67–81.

[48] Zhou AN, Sheng D, Sloan SW, Gens A. Interpretation of unsaturated soil behaviour in the stress–Saturation space, I: Volume change and water retention behaviour. Computers and Geotechnics 2012;43:178–187.

A | APPENDIX A

Flow rule parameter χ can be suitably selected to reproduce the desired total dilatancy under any given radial stress path. Consider a radial (triaxial) stress path under a constant $b_q = n_q = \dot{q}/\dot{p}$. After substantial straining the yield surface will get oriented across the imposed stress ratio $b_q = \sqrt{\frac{3}{2}\boldsymbol{b} : \boldsymbol{b}}$ and the PPS towards $d_q = \sqrt{\frac{3}{2}\boldsymbol{d} : \boldsymbol{d}}$ following equation 22. Under stabilized anisotropic conditions the model will reproduce a total dilatancy equal to $D_q = \dot{\varepsilon}_q/\dot{\varepsilon}_v = \frac{\dot{\varepsilon}_q^e + \dot{\varepsilon}_q^p}{\dot{\varepsilon}_v^e + \dot{\varepsilon}_v^p}$. Provided that total dilatancy is known, we can subtract the effect of the elastic strains to calculate a measure of the plastic deviatoric dilation d_q^p through the following expression:

$$d_q^p = D_q \left(\frac{\kappa}{\lambda - \kappa} + 1 \right) - \frac{2}{9} \cdot \frac{1+\nu}{1-2\nu} \cdot \frac{\kappa}{\lambda - \kappa} \cdot b_q \tag{34}$$

where D_q the desired total dilation and b_q the imposed stress path in the triaxial stress space.

With plastic dilation d_q^p calculated, the relative orientation of the plastic yield surface which reproduced the desired plastic dilatancy is computed, through the following quadratic equation (χ is the unknown parameter):

$$\left(\frac{2}{3}(b_q)^2 d_q^p\right)\chi^2 + \left(\frac{4}{3}b_q\right)\chi + \left(c^2 d_q^p - \frac{2}{3}(b_q)^2 d_q^p - \frac{4}{3}b_q\right) = 0 \tag{35}$$

From the two roots obtained one is usually easily rejected based on logical assumptions. The simplest way to obtain parameter χ is probably through a K_0 consolidation test. In K_0 consolidation the stress ratio b_q is directly derived from the coefficient of earth pressure at rest K_0 as $b_{q,K_0} = 3(1 - K_0)/(1 + 2K_0)$, while simultaneously the total dilatancy reproduced shall be $D_{q,K_0} = 2/3$, for the total horizontal stain to be zero. With b_{q,K_0} and D_{q,K_0} values as an input in equations 34 and 35 respectively the parameter χ is computed.